Volume Bounds for Trivalent Planar Graphs

A. Koh*

To Luke who petted Euler with me

Abstract - This paper studies the volumes of hyperbolic planar trivalent graphs. The connection between fully augmented links and trivalent planar graphs allows us to apply previous work on knots and links to this setting. Exact volume bounds for graphs with up to 12 vertices are calculated. Purcell's sharp lower bound for the volumes of fully augmented links translates directly to a lower bound for trivalent graphs. Moreover, a natural cell decomposition on trivalent graphs allows us to interpret upper bounds for link volumes in the graph theoretic setting. This is done for both the Agol-Thurston tetrahedral upper bound and Adams' bipyramidal upper bound. An infinite family of graphs, inspired by Agol-Thurston's infinite chain link fence, proves these bounds are asymptotically equivalent.

Keywords : hyperbolic geometry; graph theory; knot theory

Mathematics Subject Classification (2020) **:** 57M25; 57M50

1 Introduction

The importance of hyperbolic geometry in topology stems from Mostow's rigidity theorem, which states that in dimension at least 3, homeomorphic hyperbolic three-manifolds are isometric. Thus geometric invariants become topological ones. In particular, the importance of hyperbolic volume in topology is that each hyperbolic knot and link is associated with a unique volume which can be used as an invariant to identify properties of that knot or link.

There are many different upper bounds on volume in hyperbolic geometry for different types of hyperbolic links. A three-manifold is hyperbolic if it admits a hyperbolic metric. A link is hyperbolic if its complement is a hyperbolic manifold (see [4] for more details).

If L is an (alternating) link in S^3, Agol and Thurston use hyperbolic tetrahedra to prove (in the appendix of [7]) that

$$\mathrm{vol}(S^3 \setminus L) \leq 10v_3\ (\mathrm{t(D)} - 1),$$

where t(D) is the number of twist regions (refer to Section 2 for a definition of twist regions) and v_3 is the volume of a regular ideal tetrahedron.

A second upper bound is given by Adams [1], who who uses bipyramids to bound the volume of hyperbolic alternating links via

*This work was supported by a NSF research grant 1758020

$$\text{vol}(S^3 \setminus L) \leq \sum b_i \text{ vol}(B_i) - a.$$

The terms in Adams' upper bound refer to components of which are used to determine the upper bound – b_i being faces, B_i are i-sided bipyramids, and a being the maximum possible volume collapsed. Refer to Section 5.2.2 and [1] for more detail.

His upper bound, to be described later, improves upon that of Agol-Thurston because bipyramids have less volume than the corresponding tetrahedral decomposition.

One natural generalization of links is embedded graphs in S^3. Heard, Hodgson, Martelli and Petronio initiated a study of trivalent graphs embedded in 3-manifolds, classifying the simplest ones (see [5]). The overarching focus of this paper is to use Adams' bipyramid construction to bound volumes of planar trivalent graphs that are hyperbolic. As with links, a trivalent graph is hyperbolic if its complement admits a hyperbolic metric.

The words *trivalent*, *cubic*, and *3-regular* are words to describe graphs where each vertex has degree 3, but trivalent shall be used throughout this paper.

Masai made a connection between planar trivalent graphs in S^3 and FALs, and considered upper bounds for volumes of such graphs (see [8]). Here we extend Masai's investigation by combining his results with Agol-Thurston, Adams and Purcell. More precisely sections 2 and 3 describe fully augmented links and planar trivalent graphs. Their respective cell decompositions are described, leading to a correspondence between the two contexts. Section 4 calculates exact volumes for planar trivalent graphs of at most 12 vertices.

Section 5 focuses on volume bounds for planar trivalent graphs, in particular we find

1. sharp lower bounds for such graphs,

2. two upper bounds for volumes of these graphs and,

3. a proof that the upper bounds are asymptotically equivalent.

The lower bound is new in the graph theoretic setting, extending results in Masai [8]. Moreover, it is a direct translation of Purcell's lower bound for FAL volumes (see [9]). While Masai mentions the Agol-Thurston upper bound, this paper makes the connection more explicit by exhibiting the cell decomposition in the graph theory setting. Our application of Adams' bipiramid techniques is novel, allowing us to provide explicit examples of high-volume planar trivalent graphs.

2 FALs and Cell Decomposition

Before discussing FALs or fully augmented links, some definitions are needed.

Definition 2.1 *A twist region of a link diagram is a portion of the diagram containing only two twisted strands.*

A local picture of twists is given in Figure 1. The link diagram on the left of Figure 2 has three twists, while that on the right has four.

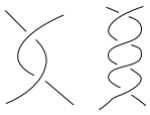

Figure 1: Left: 1 full twist. Right: 2 full twists

Definition 2.2 *A link diagram is twist reduced when all twists for a collection of knot strands are grouped in a single region.*

Figure 2 depicts two diagrams of the same link. The right diagram is not twist reduced. The two crossing twists can be flyped to join the single crossing on the left.

Figure 2: Left: twist reduced link. Right: not twist reduced link.

Definition 2.3 *A fully augmented link (FAL) is obtained from a twist reduced link by placing a trivial component around each twist region and removing full twists.*

This process is depicted in the first three pictures of Figure 3. The trivial components introduced are called crossing circles while those from the original link are called knot circles. The fourth picture indicates how each FAL can be described via painted planar trivalent graphs. Each crossing circle becomes a painted edge and each knot arc between crossing circles becomes an unpainted edge. See Purcell [9] for more about FALs.

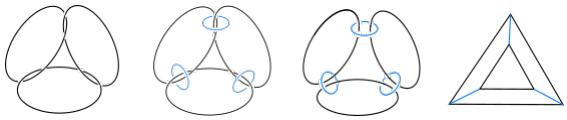

Figure 3: Example of turning link into FAL and its corresponding graph

Beginning with a topological space (like an FAL complement), one can realize a hyperbolic structure on it in the following way. Let M be a three-manifold, and choose a cell decomposition consisting of vertices (0-cells), edges (1-cells), faces (2-cells), and balls (3-cells). Slice along the faces of the cell decomposition to cut M into pieces homeomorphic to 3-cells $F_1, \ldots, F_n$, keeping track of how to glue the faces to piece M back together. Now realize each 3-cell F_i as a polyhedron in hyperbolic space. Think of these as your hyperbolic building blocks, and the gluing instructions on them tell you how to stack them together to get M. As long as some technical restrictions are satisfied (which make sure the blocks fit together nicely around edges and at corners), this places a hyperbolic structure on M (see Bonahon [4] for a nice exposition). We now apply this technique to FAL complements.

To see the hyperbolic structure on an FAL complement we describe a cell decomposition of $S^3 \setminus L$. The components of the cell decomposition of an FAL are illustrated in the leftmost picture of Figure 4.

There are two types of 2-cells, which we describe first.

Definition 2.4 *Each crossing circle bounds a disk that is punctured twice by knot circles. These are called* crossing disks.

Definition 2.5 *The knot circles cut the projection plane into pieces which make up the second kind of 2-cell, called* planar disks.

The planar and crossing disks meet orthogonally, and their intersections form the edges, or 1-cells, of the cell decomposition. Note that the endpoints of these edges lie on the FAL, so not in its complement. Hence there are no 0-cells. Finally there are two 3-cells $\mathbf{B}^3_\pm$ corresponding to the regions above and below the plane of projection. We summarize this below.

- 0-cells: None, since the endpoints of edges correspond to ideal points.
- 1-cells: Intersections of planar and crossing disks.
- 2-cells: The crossing disks, and planar disks.
- 3-cells: Everything above and below the projection plane, $\mathbf{B}^3_+$ and $\mathbf{B}^3_-$.

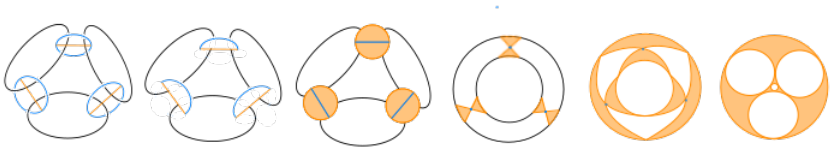

Figure 4: Polyhedral decomposition of an FAL

By the symmetry inherent in an FAL, note that the cell decomposition on $\mathbf{B}^3_-$ is the reflection of that on $\mathbf{B}^3_+$ across the projection plane. This cell decomposition can be used to obtain the polyhedral decomposition of an FAL. The following steps are illustrated in the middle 4 pictures of Figure 4.

1. Slice along planar two cells separating $\mathbf{B}^3_\pm$. Since $\mathbf{B}^3_+$ and $\mathbf{B}^3_-$ are reflections of one another across the projection plane, let's focus on $\mathbf{B}^3_+$
2. Slice crossing disks along the 1 cells and flatten out.
3. Shrink crossing arcs, so now the crossing disks look like bow ties.

4. Shrink knot arcs.

The significance of the rightmost diagram of Figure 4 is that it can be used to describe a right-angled ideal polyhedron P_+. Indeed, the unshaded faces of the diagram can become a circle packing in which all shaded regions are triangular (see Figure 5a). Purcell in [9] (see Figure a) shows how this determines a right-angled ideal polyhedron. The polyhedron P_- is obtained in an analogous way, and the link complement is achieved by gluing P_+ and P_- together, as seen below.

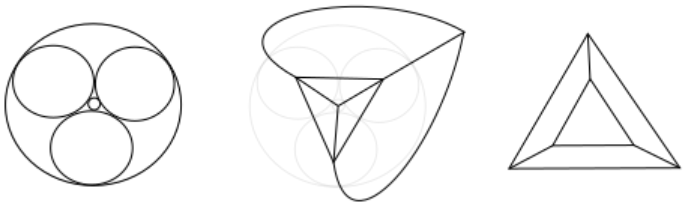

Figure 5: Left to right: a) circle packing b) nerve graph c) dual graph

There are two combinatorial ways to describe this polyhedral decomposition. The first way is the *nerve* which is a graph composed of triangular faces. Each vertex represents the center of circles in the circle packing and all edges represents the points of tangency between the circles, see Figure 5b. Another way to represent the polyhedral decomposition is the *dual* to the nerve. The *dual* of a planar graph has a vertex on each face of the original graph and vertices connected by edges going through the original graph's edges (see Figure 5c). Since the nerve is a triangulation of S^2, its dual will be a planar trivalent graph.

Figure 6: Examples of perfect matchings on the 6-vertex graph

The hyperbolic geometry of FALs, then, can be conveniently described using planar trivalent graphs. This process can be reversed provided one properly "colors" edges on a planar trivalent graph. It turns out the coloring of a dual corresponds to a perfect matching of the dual.

Definition 2.6 *A matching in a graph is a subset of edges in which no two edges have a common vertex. The two vertices of an edge in a matching can be thought of as matched or paired. A perfect matching in a graph is a matching in which every vertex is paired to another.*

Examples of perfect matchings in a dual are seen in Figure 6 as colorings of the dual. Perfect matchings are the *well-painted* graphs of Purcell [9], who shows they correspond to FALs. An example of a colored graph and its FAL can be seen in Figure 3.

3 Planar Trivalent Graphs and Cell Decomposition

This section makes the connection between fully augmented links and graphs precise. We have already seen that planar trivalent graphs arise naturally in the FAL setting as the duals to nerves of the circle packing. More generally, trivalent graphs embedded in 3-manifolds have been studied independently of FALs. Suppose we are given a trivalent graph G embedded in a 3-manifold M. Heard, et al, observe that when the complement $M \setminus G$ admits a hyperbolic structure in which meridians of edges of G are parabolic isometries, then $M \setminus G$ is a hyperbolic manifold with boundary consisting of thrice-punctured spheres (see [5]). In the case where M is the three-sphere and G is a planar trivalent graph, then $M \setminus G$ turns out to be obtained from an FAL complement by slicing along all crossing disks.

We begin this section with relevant definitions. A cell decomposition on $M \setminus G$ is then described, and the resulting polyhedra are shown to be equivalent to those described for FALs in the previous section.

Definition 3.1 *The medial graph G_m of a graph G, is defined to have midpoints of edges of G as vertices, with edges connecting midpoints of adjacent edges.*

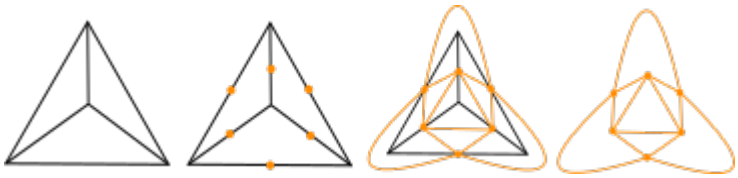

Figure 7: Creating a medial graph: place vertices on midpoints of edges, connect midpoints of adjacent edges.

The medial graph G_m of a planar trivalent graph G cuts the plane into regions that can be checkerboard colored so that each shaded face is triangular. The shaded triangles contain the vertices of the original graph G.

There is a connection between the checkerboard coloring of G_m and circle packings of FALs. More precisely the unshaded regions of G_m can be isotoped to a circle packing and the shaded triangles become the shaded regions of the circle packing.

Figure 8: Dual, dual's medial graph, and circle packing

Recall that Heard, et al, show that under certain circumstances $M \setminus G$ is a hyperbolic manifold with boundary, whose boundary is comprised of thrice-punctured spheres. Each thrice-punctured sphere in the boundary of $M \setminus G$ can be visualized on the graph at each

vertex. A sphere encircles each vertex and the edges radiating from the vertex creating three punctures in the sphere.

Thus when studying planar trivalent graphs embedded in three manifolds it is natural to consider replacing vertices with thrice-punctured spheres. Moreover, Masai and Hodgson [6] observe that planar trivalent graphs embedded in S^3 give rise to FALs by appropriate gluings on the thrice-punctured sphere boundary components. Rather than rely on Masai's observations [8], we directly describe a cell decomposition on planar trivalent graphs in S^3 (with thrice-punctured spheres surrounding the vertices). This cell decomposition will give rise to right angled ideal polyhedra $P_\pm$ analogous to the FAL setting. The resulting components of the cell decomposition of a trivalent planar graph are

- 0-cells: None, since ideal polyhedrons are used
- 1-cells: Intersection of the spheres with the plane
- 2-cells: The thrice-punctured spheres and the planar regions
- 3-cells: The regions above and below the plane, B_+ and B_-

To obtain a cell decomposition of a planar trivalent graph, refer to Figure 9: Let G be a planar trivalent graph with each vertex replaced with a thrice-punctured sphere. To see the hyperbolic structure on a $S^3 \setminus G$, slice along the planar two-cells to separate it into two pieces. Focusing on the top half, the sliced thrice-punctured spheres form triangles and edges of G surround planar regions. Shrinking edges of G to points results in a checkerboard colored cell decomposition where the unshaded faces can form a circle packing. As in the FAL setting these can be realized geometrically as polyhedra $P_\pm$. In this setting, gluing only unshaded faces, and leaving shaded triangles above them, yields $S^3 \setminus G$. Comparing this construction with the hyperbolic structure on an FAL complement shows that $S^3 \setminus G$ is an FAL sliced along its crossing disks.

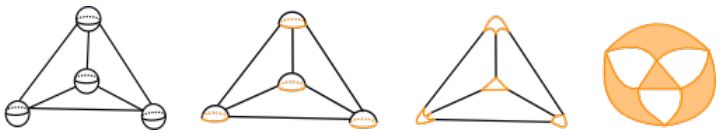

Figure 9: Cell decomposition of the planar graph

4 Exact Volumes

Now that we have an explicit construction for the hyperbolic structure on the complement of planar trivalent graphs in S^3, let's proceed with explicit volume calculations for graphs with few vertices. The goal for this section is to compute exact volume upper bounds for graphs with up to twelve vertices.

Let's begin with an example which walks through the process of finding the volume of a graph, referring to Figure 10.

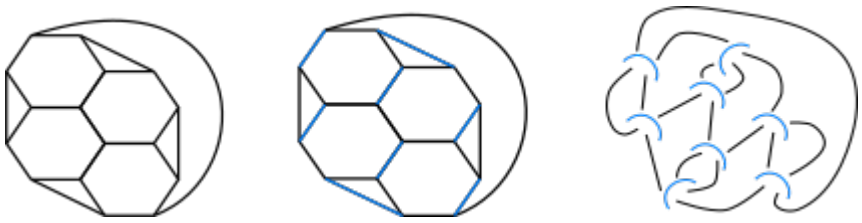

Figure 10: Dual graph and conversion to FAL

We start with the trivalent planar graph whose volume we want to find. In the middle image we color the graph with a perfect matching. We use the coloring to find the corresponding FAL, colored edges turning into trivial crossing circles (depicted as half arcs), and the uncolored edges becoming knot arcs as seen on the right. The FAL is then drawn in *SnapPy* [10] and we use the program to calculate the volume (see Figure 11). *SnapPy* is a program that was also used by [5] to calculate the volumes of hyperbolic graphs. As you can see, the volume of this particular graph is 53.403.

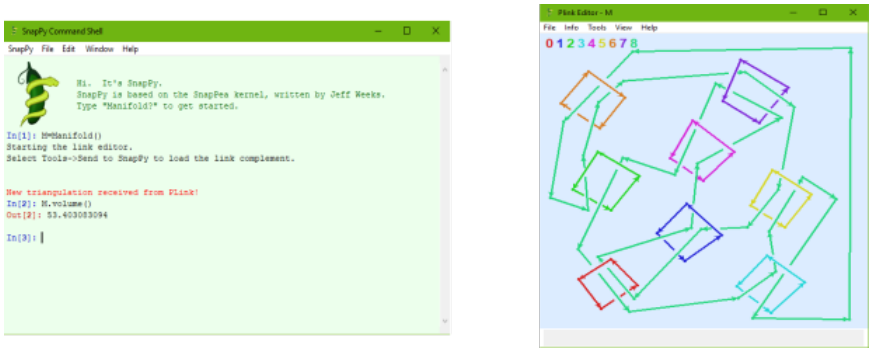

Figure 11: Drawing FAL into SnapPy

This process is repeated for several small trivalent planar graphs. Using a table of simple trivalent graphs [11] we determined which are planar. To find the volume of planar ones, we used perfect matchings to find associated FALs, then used the *SnapPy* program to compute the volume. This method is limited in that after 12 vertices, there are too many graphs to find volumes by hand, and by the fact that *SnapPy* is restricted on the number of components it can manage. The calculated maximum volume for graphs is compared with Agol-Thurston's bound and with Adam's collapsed bipyramidal construction below. This table coincides with and extends Masai's calculations in [8]. Notice that the table of Figure 12 only contains graphs with an even number of vertices. We leave it as an exercise for the reader to confirm that all planar trivalent graphs have an even number of vertices.

Vertices	Maximum Volume	Agol-Thurston	Adams
4	7.3277	10.1494	8.1192
6	14.6554	20.2988	15.8426
8	24.0922	30.4482	24.1882
10	32.5515	40.5676	35.8803
12	41.4162	50.747	45.8095

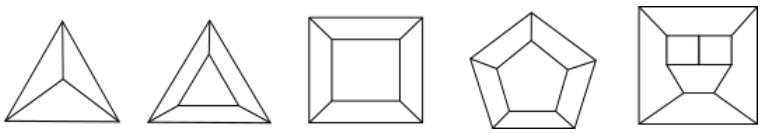

Figure 12: The maximum volume graphs in ascending vertex count order.

There are unique 4-vertex and 6-vertex trivalent planar graphs, which makes it easy to compute the maximum (and minimum) volume. To obtain the maximum volume for 8- and 10-vertex graphs, we compiled an exhaustive list, computing all volumes, to obtain the maximum volume. There are too many 12-vertex trivalent planar graphs for the exhaustive approach to be feasible. Instead we used a relationship between edge connectivity and volume to find a volume upper bound in this case.

Let G be a trivalent planar graph in S^3 such that $M = S^3 \backslash G$ has a hyperbolic structure with parabolic meridians. If G has a 3-cut (three edges whose removal separates G into two non-trivial graphs), it turns out vol(M) decomposes in a nice way.

More precisely, there is a sphere S in S^3 intersecting G in three points, one point on each edge of the 3-cut (see dotted line in Figure 13). In M then, S is a sphere with three punctures - a thrice-punctured sphere. Adams work from [1] implies that any such thrice-punctured sphere S in M is is totally geodesic, so one can slice along it and get two manifolds, whose volumes add to the volume of the original manifold. Moreover, slicing along S just creates 2 new trivalent planar graphs by considering the copies of S to be thrice-punctured spheres around new vertices (see the bottom row of Figure 13).

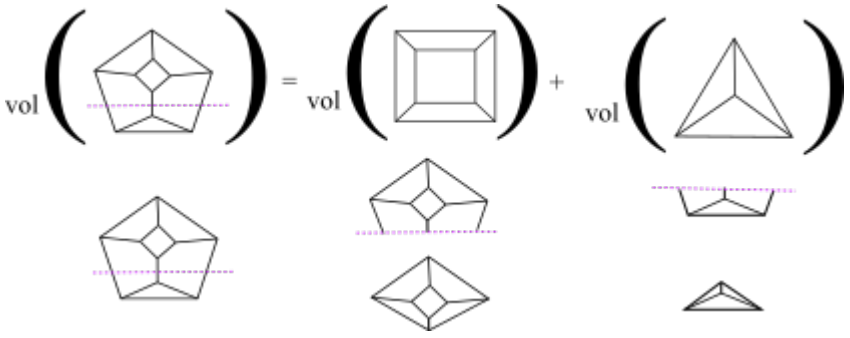

Figure 13: Slicing and 10 vertex graph along a 3-cut. Cut edges are joined at a new vertex. So the volume of the 10 vertex graph is the sum of the 2 prime graphs.

The purpose of this discussion is the following observation.

Lemma 4.1 *If G is a n-vertex hyperbolic planar trivalent graph in S^3 containing a 3-cut, then there are hyperbolic trivalent planar graphs G_1 and G_2 with n_1 and n_2 vertices satisfying*

$$vol(S^3 \setminus G) = vol(S^3 \setminus G_1) + vol(S^3 \setminus G_2),$$

where $n_1 + n_2 = n + 2$.

Proof. Since G has a 3-cut , $S^3 \setminus G$ contains a thrice-punctured sphere S and shows the existence of G_1, G_2. Moreover, slicing along S produces two additional vertices, proving $n_1 + n_2 = n + 2$. □

Note that the maximum-volume trivalent planar graphs with at most 10 vertices are 4-connected. In other words, they have no 3-cuts. Motivated by this observation, we focused on calculating the volumes of 4-connected 12-vertex graphs, of which there are only two (see graphs 12.1 and 12.2 in Figure 14).

Lemma 4.2 *The maximum volume of a 12-vertex hyperbolic planar graph is 41.4162.*

Proof. To see this, compare the maximal calculated volume 41.4162 to the volumes of 12-vertex graphs with a 3-cut. By Lemma 4.1, this amounts to summing volumes of two graphs whose vertices add up to $n_1 + n_2 = 12 + 2 = 14$. This sum is at most the sum of the upper bounds we have already found corresponding to n_1- and n_2-vertices. A quick check of the appropriate values in Figure 12 show these sum to less than 41.4162. □

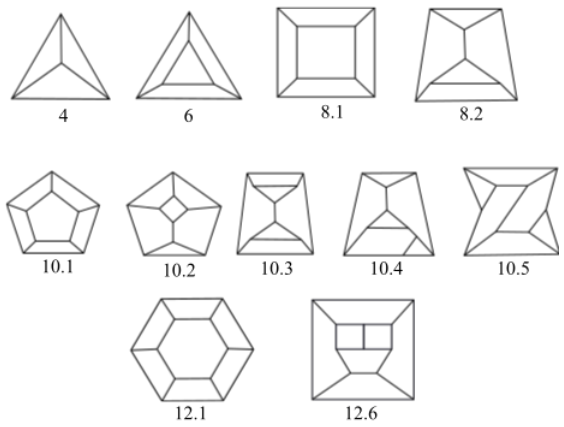

Figure 14: The following table's planar trivalent graphs.

In the following table the graphs are denoted by their labeling in Figure 14. Each planar trivalent graph decomposes the plane into polygons. The next four columns record how many polygons of a certain number of edges arise. These faces are used to help determine the uncollapsed bipyramidal volume, which is an upper bound for the planar trivalent graphs and is described in Section 5.2. The final column calculates the bipyramidal upper bound volume without collapsing. The computed volumes clearly show that

the actual volume of the graphs are always lower than the uncollapsed bipyramidal bound on volume.

Graph	3-edged face	4	5	6	Volume	Uncollapsed Bipyr Vol
4	4	0	0	0	7.3276	16.2384
6	2	3	0	0	14.6552	27.2298
8.1	0	6	0	0	24.0921	38.2212
8.2	2	2	2	0	21.98	37.599
10.1	0	5	2	0	32.5515	48.5904
10.2	1	3	3	0	31.4199	48.2793
10.3	2	3	0	2	29.3109	47.5282
10.4	3	0	3	1	29.3109	47.4371
10.5	2	2	2	1	29.3109	47.7482
12.1	0	6	0	2	40.5977	58.5196
12.2	0	4	4	0	41.4162	58.9596

5 Volume Bounds

In this section we provide both lower and upper bounds for volumes of hyperbolic planar trivalent graphs. The lower bound is a direct consequence of Purcell's work on FALs. We present two upper bounds, translating the work of Agol-Thurston and Adams into the graph theoretic setting. Finally, we construct examples that show the upper bounds are asymptotically sharp.

5.1 Lower Bound

A lower bound for volumes of hyperbolic FALs appears in [9], in which Proposition 3.6 states

Proposition 5.1 (Purcell) *If L is a hyperbolic fully augmented link with c crossing circles, then*

$$vol(S^3 \setminus L) \geq 2v_8(c - 1)$$

where $v_8 = 3.66386...$ is the volume of a regular ideal octahedron. Moreover

$$vol(S^3 \setminus L) = 2v_8(c - 1)$$

if and only if $S^3 \setminus L$ decomposes into regular ideal octahedra.

Recall that a perfect matching on a trivalent planar graph G corresponds to an FAL with the same volume (see Figure 13). In particular, note that crossing circles in the FAL correspond to pairs of vertices that are matched in G.

Given any trivalent planar graph G with V vertices, then one can construct an FAL with the same volume and $\frac{V}{2}$ crossing circles, see Figure 10 to compare vertices and

crossing circles. Thus a lower bound on the volumes of FALs also gives a lower bound on volumes of graphs. Hence any hyperbolic planar trivalent graph G satisfies

$$\begin{aligned} vol(S^3 \setminus G) &\geq 2v_8 \left(\frac{V}{2} - 1 \right) \\ &= v_8(V-2) \end{aligned}$$

Purcell's bound is sharp and we summarize Purcell's construction.

A central subdivision of a triangular face in the nerve corresponds to adding a vertex inside a face and connecting it to the original vertices (compare graphs labeled "nerve" in Figure 15).

Purcell observes that each successive central subdivision of a triangle within the nerve adds a circle in one of the shaded triangles in the nerve's circle packing. The adding of a circle in a triangle of the circle packing is the same as adding an ideal regular octahedron. This result is not immediately obvious, and verifying it would take us too far afield. We refer the interested reader to Section 3.3, and more specifically Proposition 3.8, of [9] for a thorough treatment. By repeatedly adding regular ideal octahedra, then, one can construct FALs with the desired volume.

To see that Purcell's (see Figure 15 and the proof of [9, Prop 3.8]) lower bound is sharp for planar trivalent graphs, one need only translate what central subdivisions in the nerve correspond to in the dual. The central subdivision of a nerve is equivalent to turning a vertex of the trivalent graph into a triangle. Indeed, the triangular face in the original nerve corresponds to a single vertex in the dual. Centrally subdividing that face corresponds to a triangle in the dual (compare graphs labeled "dual" in Figure 15). Thus beginning with K_4 and repeatedly replacing vertices with triangles yields trivalent planar graphs whose volumes are $v_8(V-2)$.

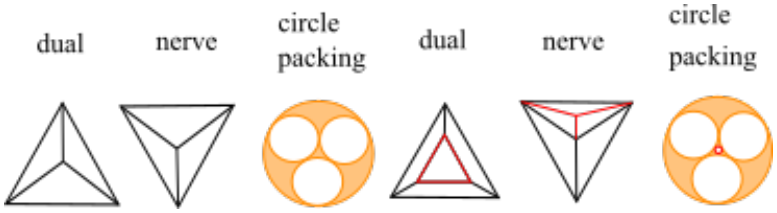

Figure 15: The effect of centrally subdividing a nerve on its dual and corresponding circle packing.

The above argument proves the following:

Proposition 5.2 *If G is a hyperbolic planar trivalent graph with V vertices then*

$$vol(S^3 \setminus G) \geq v_8(V-2).$$

Moreover, this lower bound is sharp.

5.2 Upper Bounds

We now will apply techniques for finding upper bounds on volumes of hyperbolic links to the trivalent graph setting. In particular, we will translate both Agol-Thurston's tetrahedral upper bound and Adams' bipyramid construction to trivalent planar graphs. Recall that v_3 is the volume of an ideal regular tetrahedron.

5.2.1 Agol-Thurston's Upper Bound

Agol-Thurston improved Lackenby's [7] upper bound for the volume of links with a prime alternating diagram. Their result was

Theorem 5.3 (Agol-Thurston) *Given a projection diagram D of a link L with twist number $t(D)$ then*

$$vol(S^3 \setminus L) \leq 10v_3(t(D) - 1).$$

Moreover there is a sequence of links L_i such that

$$vol(S^3 \setminus L)/t(D_i) \to 10v_3.$$

Overview of Proof
Given an alternating link L, Agol-Thurston prove their theorem by first creating an augmented alternating link A_L then cellularly decomposing it in a slightly different way from Section 2. We shall call the decomposition here tetrahedral decomposition. Choose a point v_+ interior to P_+ and connect each ideal vertex to it. Likewise, choose a point v_- interior of P_- and perform the same construction. The result is that tetrahedra are then placed on each shaded region, one each on P_+ and P_-. Noting that each twist region of L yields a crossing circle of A_L, which decomposes into 2 shaded regions, there are $4t(D)$ tetrahedra on the shaded regions. The unshaded faces have two pyramids on them - one in P_+ and P_-. The pyramids are divided into as many tetrahedra as it has sides by stellar subdivision (see rightmost picture in Figure 16).

A stellar subdivision of an unshaded face F is obtained as follows. Connect vertices $v_\pm$ with an edge through face F. The vertices of every edge in the boundary of F combine with $v_\pm$ to form a tetrahedron. The union of these tetrahedra over all edges of F form the stellar subdivision of the two pyramids on F.

Noting that there are $2t(D)$ shaded faces, each with 3 edges, we can see there are $6t(D)$ edges in the tetrahedral cell decomposition. Since each edge contributes one tetrahedron through an unshaded face, the number of tetrahedron given by the unshaded faces is $6t(D)$. Hence, the total number of tetrahedra so far is $10t(D)$. Now Agol-Thurston collapse tetrahedra. To collapse tetrahedra, pick an ideal vertex w. Shrink the edges joining w to $v_\pm$, carrying the entire cell decomposition along in the shrinking process. This process collapses all tetrahedra on the four faces adjacent to w, and leaves the remaining tetrahedra. Since every 2 unshaded regions have at least 6 tetrahedra and every 2 shaded regions have 4, we may collapse 10 tetrahedra, resulting in

$$vol(S^3 \setminus A_L) \leq 10v_3(t(D) - 1).$$

The above holds since the maximum volume of a hyperbolic tetrahedron is v_3 and realized by a regular ideal tetrahedron. See Theorem C.2.1 of Benedetti-Petronio [3].

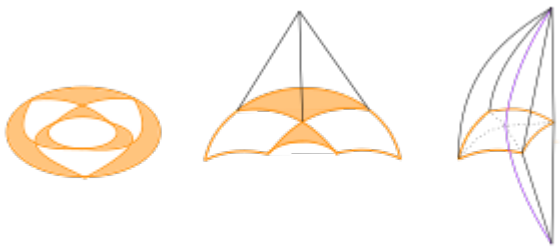

Figure 16: Placement of tetrahedra on shaded regions and stellar subdivision of unshaded regions into tetrahedra.

The original link L is obtained by Dehn filling A_L, which always reduces volume so

$$vol(S^3 \setminus L) \leq 10v_3(t(D) - 1)$$

For more detail, please view Agol-Thurston's proof in full in their appendix to Lackenby [7].

The difference between this tetrahedral cell decomposition and that of Section 2 is that Section 2 is satisfied with constructing right-angled ideal polyhedra while the tetrahedral cell decomposition needed to decompose them into ideal tetrahedra for their volume bound. Thus the tetrahedral cell decomposition construction uses the same 2-cells as Section 2, it just further decomposes $P_\pm$ into tetrahedra.

The Agol-Thurston upper bound for volume on the FAL $\mathcal{A}_L$ translates immediately to an upper bound on the volumes of trivalent planar graphs. Given a hyperbolic trivalent planar graph G we've seen that it's complement is obtained by gluing two right-angled ideal polyhedra $P_\pm$ together along their unshaded faces. Using the tetrahedral procedure further decomposes $P_\pm$ into tetrahedra, so their upper bound applies in the graph setting as well.

We now complete the translation of the Agol-Thurston upper bound to the graph setting. Recall that there is one vertex of G for every shaded triangle in the cell decomposition of an associated FAL, and two shaded triangles in an FAL for every twist region in a diagram; thus $t(D) = V/2$. This discussion proves:

Theorem 5.4 *Given a hyperbolic trivalent planar graph G with V vertices,*

$$vol(S^3 \setminus G) \leq 10v_3 \left(\frac{V}{2} - 1 \right).$$

5.2.2 Adam's Upper Bound

Adams improved on the Agol-Thurston upper bound for hyperbolic alternating links using a bipyramidal construction. An *n-sided bipyramid* is an ideal polyhedron obtained by gluing n ideal tetrahedra in a cycle around a common edge. Bipyramids arise in the tetrahedral decomposition when considering the unshaded faces in $P_{\pm}$. Agol and Thurston place a pyramid on each unshaded face, so when gluing they become bipyramids. Agol and Thurston decompose these bipyramids into tetrahedra using stellar subdivision. The difference with Adams' bipyramids is that stellar subdivision is unecessary in the unshaded faces of the polyhedral decomposition. By using bipyramids through the faces of the augmented link instead of stellar subdivisions the process is much more efficient, since the volume of an n-sided bipyramid is always less than the volume of the sum of n tetrahedra. Refer to Adams [1] for more detail on his upper bound for hyperbolic alternating links.

Figure 17: The upper halves of bipyramids and local collapsing.

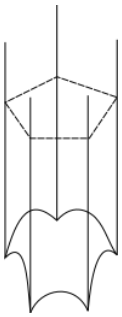

Figure 18: An ideal bipyramid with edges going to infinity, the dotted line showing where the projection plane intersects.

In Figure 17, the upper halves of bipyramids are displayed on the polyhedral cell decomposition. Again choose a point in P_+, and another P_- interior to the polyhedra. Coning those points to every vertex in the cell decomposition results in a bipyramid corresponding to every face. The first image in Figure 17 displays only the top half of the bipyramids for clarity. At this stage of Adams' construction the bipyramids are coned to finite vertices rather than ideal ones. Adams, as with Agol-Thurston, then picks one ideal vertex and shrinks the edge connecting it to the finite vertex, carrying all edges along the process. The second image of Figure 17 displays the regions around a chosen ideal point. The third displays shrinking the edge at that ideal point and the flattening of adjacent

faces that results from it. This collapsing at the ideal point also happens in the lower half.

Adams' upper bound would then be defined as the bipyramidal upper bound:

Theorem 5.5 (Adams) *Given a projection diagram D of a hyperbolic link L which decomposes the projection plane into b_i i-gons,*

$$vol(S^3 \setminus L) \leq \sum b_i vol(B_i) - k,$$

where b_i is the amount of bipyramids with i sides, and B_i is the regular ideal bipyramid with i-sides that maximizes volume. See [1] theorems 4.1 and 2.1 for more details.

Here k is the the volume of the two 3-sided bipyramids on the unshaded faces at the chosen ideal point that collapse during the shrinking process. This k-value relates to the a-value in Adams paper, but is more easily determined. The above theorem's k-value pertains to the FAL decomposition case and is determined by selecting the largest adjacent unshaded faces that meet at the ideal point (see [1] for more detail).

As with the Agol-Thurston cell decomposition, Adams' bipyramid construction can be obtained by further subdividing the $P_\pm$ of Section 2. His upper bound, then, immediately translates into the graph setting.

Theorem 5.6 *Given a hyperbolic trivalent planar graph G with V vertices that decomposes the plane into b_i i-gons, then*

$$vol(S^3 \setminus G) \leq \Sigma b_i vol(B_i) + (V-2)vol(B_3)$$

Proof. Each vertex of G corresponds to a shaded triangle in the cell decomposition, yielding a B_3 bipyramid. Since two of these collapse, we get $(V - 2)$ of them. Secondly, since each i-gon of G contributes an unshaded i-gon to the cell decomposition, the summation is that of Adams' theorem. □

Note that in Adams' construction you can choose which ideal vertex to collapse toward. He chooses to collapse to the vertex whose unshaded regions contribute the most volume to his upper bound. The sum on the right does not include the volumes from these two bipyramids. For simplicity, we let

$$BUB = \Sigma b_i vol(B_i) + (V-2)vol(B_3)$$

represent the "Bipyramid Upper Bound" for the volume of $S^3 \setminus G$.

Remark 5.7 Note that by construction Adams' upper bound is lower than the Agol-Thurston upper bound. Adams' bound is lower than Agol-Thurston's bound because n-sided regular ideal bipyramids have less volume than n regular ideal tetrahedra. Agol-Thurston have shown their upper bound to be asymptotically sharp. They do this by constructing an infinite family of links with volumes approaching their bound. Since Adams' bipyramid bound is lower than the Agol-Thurston bound, it must be asymptotically sharp as well.

By revisiting the example of the exact volume of a graph calculated in Section 4, we shall walk through the process of obtaining the bipyramidal upper bound volume of the graph in Figure 19.

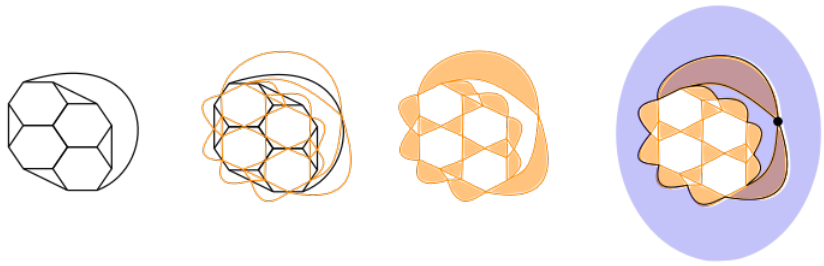

Figure 19: From left to right: the 16 vertex hexagonal graph, cellular decomposition via medial graph, circle packing, blue shaded regions are what is eliminated surrounding the black dot which is chosen as the vertex to collapse

First each face is either a triangle or a hexagon. Counting the number of each type, we see within the dual:

Number of Edges Bounding	3	6
Number of Faces	4	6

Recalling that the medial graph corresponds to the polyhedral decomposition, we see that each vertex in the dual corresponds to a three-sided face on the boundary of P±. So adding the number of vertices, 16, informs that the polyhedral decomposition has:

n-Sided Face	3	6
Number of Faces	20	6

Now we must collapse the two largest faces, which share the line that arcs around half the graph. In this example the two largest faces are both 6-sided. We must also collapse the bipyramids on the two adjacent shaded faces. This results in a final bipyramid count of

n-Sided Bipyramid	3	6
Number of Bipyramids	18	4

Noting that the volume of a 3-sided bipyramid is 2.0298 and a 6-sided bipyramid is 6.0896 for regular ideal bipyramids (see Table 1 from [1]) then the bipyramidal volume upper bound is

$$\begin{aligned} 18vol(B_3) + 4vol(B_6) &= 18 * 2.0298 + 4 * 6.0896 \\ &= 60.8948 \end{aligned}$$

Calculations similar to this, but without the collapsing, were used to complete the table of Section 4.

5.2.3 Putting Together Agol-Thurston and Adams

Agol-Thurston show their upper bound is asymptotically sharp by doing complex polyhedral gluings on the infinite chain link fence. Since Adams' bound is lower, this proves it is asymptotically sharp for links as well. A priori, our translation of Adams' bound to trivalent graphs could be asymptotically lower than that of Agol-Thurston. We prove that this is not the case, rather the two bounds are asymptotically equivalent.

Theorem 5.8 *Given a planar trivalent graph G having V vertices and bipyramidal upper bound (BUB)*

$$BUB \leq 10v_3(\tfrac{V}{2} - 1).$$

Moreover there is a sequence of graphs G where

$$BUB/\tfrac{V}{2} \to 10v_3.$$

Proof. To prove the asymptotic result we note that Agol-Thurston's infinite chain-link fence translates into a hexagonal tesselation of $\mathbb{R}^2$ in the trivalent graph setting. We choose a finite approximation H_m of the hexagonal tesselation for every even m ≥ 4 (see Figure 20).

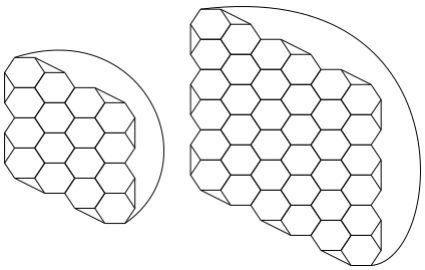

Figure 20: Finite approximations of the infinite chain-link fence.

The graph H_m cuts the plane into polygonal faces. To compute $BUB(\mathrm{H}_m)$ we begin by counting the number of faces of each type. It can be noted that there are m^2 hexagonal faces. There are also 2m triangular faces, and two 3m-sided faces (the largest faces). Recall Adam's bipyramidal construction in Section 5.2.2., in which collapsing the largest faces results in the least upper bound for the bipyramid construction. We will be collapsing the 2 largest faces since their sharing of an edge in the planar trivalent graph translates to an ideal point in the FAL's cell decomposition.

To complete our calculation of BUB(H_m) we also need the number of vertices, which will each have a 3-sided bipyramid through them (except for the 2 collapsed at the ideal point). To obtain this number, we shall utilize the Euler characteristic and the graph's trivalent property. The graph H_m gives a cell decomposition of S^2, so the number of vertices, edges and faces satisfies V - E + F = 2. Moreover, a trivalent graph has degree three on each vertex, and summing the degrees of the vertices counts each edge in a graph twice, allowing us to see that 3V = 2E.

Thus by substituting, we have

$$\begin{aligned} V - E + F &= 2 \\ V - \frac{3V}{2} + m^2 + 2m + 2 &= 2 \\ m^2 + 2m &= \frac{V}{2} \\ 2m^2 + 4m &= V. \end{aligned}$$

Using Adams bipyramidal construction we place n-sided bipyramids on all n-sided faces and 3-sided bipyramids on all vertices. Finally we collapse the two largest faces together with the adjacent shaded triangles. We then see

$$\begin{aligned} BUB(H_m) &= m^2 vol(B_6) + (2m + 2m^2 + 4m - 2)vol(B_3) \\ &= m^2 vol(B_6) + (2m^2 + 6m - 2)vol(B_3). \end{aligned}$$

Noting $vol(B_6) = 6.0896 = 6v_3$ and $vol(B_3) = 2.0298 = 2v_3$ (see Table 1 of Adams [1]).

$$\begin{aligned} BUB(H_m) &= m^2 6v_3 + (2m^2 + 6m - 2)2v_3 \\ &= m^2 6v_3 + m^2 4v_3 + m12v_3 - 4v_3 \\ &= m^2 10v_3 + m12v_3 - 4v_3 \end{aligned}$$

To show $\mathrm{BUB}(\mathrm{H}_m)/\frac{V}{2} \to 10\mathrm{v}_3$ divide sides by $\frac{V}{2}$ and take a limit as m goes to infinity:

$$\begin{aligned} \lim_{m\to\infty} \frac{BUB(H_m)}{m^2 + 2m} &= \lim_{m\to\infty} \frac{m^2 10v_3 + m12v_3 - 4v_3}{m^2 + 2m} \\ &= 10v_3. \end{aligned}$$

This verifies the asymptotic behavior of $\mathrm{BUB}(\mathrm{H}_m)$. Since Adam's shows that his bipyramid construction is always at most the tetrahedral constant of Agol-Thurston, we also have

$$BUB \leq 10v_3(\tfrac{V}{2} - 1).$$

□

Despite supporting that $10v_3$ is an optimal coefficient to the upper bound on volume, there are still several unknowns in the bipyramidal volume construction for trivalent graphs. Since this paper works with small trivalent graphs, the hexagonal construction may not be the graph of the maximum volume for a given number of vertices.

6 Future Research

This project has suggested many questions that can be explored more extensively to find potentially lovely results.

- Is there any way to further improve the bipyramid bound? (see [7])
- What volume bounds exist for non-planar graphs?
- Show that 4-connected graphs also reach the upper bound for large enough vertices.
- Is there a lower bound for the hexagon family graphs?
- Can Lackenby's article on guts of surfaces be used to find a lower bound on the maximum volume of graphs?
- Is there a way to prove that graph connectivity is related to the graphs with maximum volume?

Acknowledgments

I would like to thank Rolland Trapp for his immense help in guiding this research and creating this paper, the whole CSUSB 2019 REU group, CSUSB for hosting the summer research, the NSF for funding this research with grant 1758020, the Pacific University math faculty, and Luke Davis for cheering me on each day. Thanks also to the referee for a careful reading and helpful suggestions, resulting in an improved version of this paper.

References

[1] C. Adams, Bipyramids and Bounds on Volumes of Hyperbolic Links, *Topology Appl.*, **222** (2017), 100–114.

[2] C. Adams, Thrice-Punctured Spheres in Hyperbolic 3-Manifolds, *Trans. Amer. Math. Soc.*, **287** (1985), 645–656.

[3] R. Benedetti, C. Petronio, *Lectures on Hyperbolic Geometry*, Springer-Verlag Berlin Heidelberg, 1992.

[4] F. Bonahon, *Low-dimensional geometry: from Euclidean surfaces to hyperbolic knots*, IAS/Park City mathematical subseries, (2009).

[5] D. Heard, C. Hodgson, B. Martelli, C. Petronio, Hyperbolic graphs of small complexity, *Experiment. Math.*, **19** (2009), 211–236.

[6] C. Hodgson, H. Masai, *On the number of hyperbolic 3-manifolds of a given volume*. Amer. Math. Soc., Providence, RI, 2013.

[7] M. Lackenby, The Volume of Hyperbolic Alternating Link Complements, *Proc. Lond. Math. Soc.*, **88** (2004), 1–30.

[8] H. Masai, On Volume Preserving Moves on Graphs with Parabolic Meridians, *Kyoto Univ. Information Repository*, **5** (2013), 88–93.

[9] J.S. Purcell, An introduction to fully augmented links, Interactions between hyperbolic geometry, *Contemp. Math. Amer. Math. Soc.*, **541** (2011), 205–220.

[10] SnapPy Software, available online at the URL: `https://www.math.uic.edu/t3m/SnapPy/`

[11] Table of simple cubic graphs, available online at the URL: `https://en.wikipedia.org/wiki/Table_of_simple_cubic_graphs`

[12] W.P. Thurston, *The geometry and topology of three-manifolds*, Princeton Univ. Math. Dept. Notes, 1979.

Anita Koh
3481 Pacific University
2043 College Way
Forest Grove, Oregon
E-mail: `koh7402@pacificu.edu`

Received: May 14, 2020 **Accepted**: July 4, 2020
Communicated by Corey Dunn